Evaluation of an Analytic Reconstruction Method as a Platform for Spectral CT

Huihua Kong[1], Rui Liu[2], Hengyong Yu[2]
1. *School of Science, North University of China, Taiyuan, Shanxi, 030051,China*
2. *Department of Electrical and Computer Engineering, University of Massachusetts Lowell, Lowell, Massachusetts, USA*
Email: huihuak@163.com, liurui1217@gmail.com, hengyong-yu@ieee.org

Abstract— **The goal of this paper is to evaluate an analytic spiral cone-beam CT (CBCT) algorithm for spectral CT to provide a fair comparison platform for the state-of-the-art iterative reconstruction algorithms. Considering the fact that a narrow energy channel has high noise which degrades the imaging quality of spectral CT, an adaptive maximum a posterior (MAP) sinogram restoration algorithm is first used to reduce the noise and then a three dimensional weighted Feldkamp-Davis-Kress (FDK) algorithm is implemented to reconstruct the spectral CT images at different energy channels. Our numerical results show that the analytic reconstruction approach is fast and it can provide high spatial resolution, high contrast resolution and high signal-noise-ratio (SNR) with higher helical pitches. This makes it possible to serve as a platform to evaluate the state-of-the-art iterative spectral CT algorithms.**

Keywords—Spectral CT, spiral CBCT, adaptive MAP, weighted FDK.

I. INTRODUCTION

Recently, spectral CT with photon-counting detector has gained considerable interests and become a hot topic [1]-[3]. The state-of-the-art photon-counting detectors usually divide the energy range of a spectrum into several channels. Because each sub-spectrum or energy channel can be used to reconstruct an image like the conventional CT, the spectral CT can be viewed as a natural extension of the conventional CT along the spectral dimension, and the additional spectral information can help to distinguish materials and improve the contrast-to-noise ratio (CNR). Unfortunately, as far as the authors know, a comprehensive evaluation of analytic reconstruction algorithms for spectral CT has not been reported. This motivates us to evaluate analytic spiral cone-beam CT (CBCT) algorithms to provide a fair comparison platform for iterative spectral CT reconstruction algorithms.

An obvious limitation of spectral CT is that the number of photons available in each energy channel is much smaller than the total number of photons detected, and image noise within each channel is dramatically increased. Consequently, how to reconstruct high quality CT images from noisy projections has recently become a hotspot in the spectral CT field. Although different algorithms have been developed to reconstruct high quality spectral CT images, there is no unique platform for performance comparison. To resolve this problem, we aim to implement and evaluate an analytic reconstruction platform. In this paper, an adaptive maximum a posterior (MAP) sinogram restoration algorithm is first implemented to reduce noise. Then, a helical weighted Feldkamp-Davis-Kress (FDK) spectral CT algorithm is employed to reconstruct images from denoised projections. Finally, comprehensive experiments are performed to evaluate the performance of this analytic reconstruction algorithm for spectral CT.

II. SPECTRAL CT DATA AND NOISE MODEL

A. Spectral CT Data

For a photon-counting detector, the comparator for each channel can be set as a threshold level. By a simple post-processing step of subtraction, the received photon intensity can be modeled for a given energy channel defined by two energy thresholds ($0 < T_1 < T_2$)

$$b(T_1,T_2)=\int_{T_1}^{T_2} b_0(E)D(E)\exp\left(-\int_L \mu(E,l)\,\mathrm{d}l\right)\mathrm{d}E \qquad (1)$$

where E is energy, $b_0(E)$ is the photon intensity emitting from the x-ray source, $D(E)$ is the detector efficiency, $b(T_1,T_2)$ is the received photon intensity by the detector, L represents the x-ray path, and $\mu(E,l)$ is the attenuation map depending on energy E .

Similar to the conventional CT, a logarithm operation can be applied to Eq.(1) to approximately obtain

$$y(T_1,T_2)=\ln\left(\frac{\int_{T_1}^{T_2} b_0(E)D(E)\mathrm{d}E}{b(T_1,T_2)}\right)\approx\int_L \bar{\mu}(\bar{E},l)\mathrm{d}l \qquad (2)$$

where $\bar{\mu}(\bar{E},l)$ denotes weighted average value of the attenuation coefficient and $\bar{E}$ denotes the equivalent energy in the interval $[T_1,T_2]$. Eq.(2) is the well-known radon transform model and it has been widely accepted in the CT field for spectral CT [4].

For a given energy channel $T_1 < E < T_2$, noisy CT sinogram measurements can be expressed as a discrete vector $\boldsymbol{y}=(y_1,y_2,\cdots,y_i,\cdots,y_I)$, where y_i represents the i^{th} line integral through the object for a given scanning geometry, and I is the number of total measurements. These measurements are

related to the recorded detector measurements, $\boldsymbol{b}=(b_1,b_2,\cdots,b_i,\cdots,b_I)$, by the Equation (2).

B. Noise Model

A poisson noise model for pre-log data b_i can be written as

$$b_i \sim Poisson\left\{b_0^i \exp\left(-\int_L \mu(\bar{E},l)\,\mathrm{d}l\right)+r_i\right\} \tag{3}$$

where b_0^i is the X-ray source intensity for i^{th} ray, and r_i denotes the background contributions from factors such as scatter and crosstalk. After a negative log operation, the post-log data y_i can be approximately viewed as a Gaussian random variable [5]. The relationship between the data mean and variance is described by

$$\sigma_i^2 = f_i \exp(y_i/\eta) \tag{4}$$

where y_i and σ_i^2 are the mean and variance of the i^{th} ray integral, f_i is a parameter adaptive to detector bins and η are scaling parameter which is object-independent but completely determined by the system settings.

III. Adaptive MAP Sinogram Restoration

Image restoration problem of spectral CT projection for each channel can be formulated as a minimization problem [5], and it also can be considered as an MAP with a quadratic prior potential function estimation of the noisy sinogram

$$\hat{\boldsymbol{p}} = \arg\min_{\boldsymbol{p}}\left(\sum_{i=1}^{I}\frac{(y_i-p_i)^2}{2\sigma_i^2}+\beta\frac{1}{2}\sum_{i=1}^{I}\sum_{j\in N_i}\omega_{ij}\left(p_i-p_j\right)^2\right). \tag{5}$$

The iterative updating formula for the solution of (5) by the Gauss-Seidel algorithm is given by [6]

$$p_i^{(n+1)} = \frac{y_i+\beta\sigma_i^2\left(\sum_{j\in N_i^1}\omega_{ij}p_j^{(n+1)}+\sum_{j\in N_i^2}\omega_{ij}p_j^{(n)}\right)}{1+\beta\sigma_i^2\sum_{j\in N_i}\omega_{ij}}, \tag{6}$$

where n represents the iterative number , N_i represents a neighborhood of six nearest volxels centered on p_i , N_i^1 denotes the upper, left and front neighbors, N_i^2 denotes the lower, right and back neighbors, and ω_{ij} is the smoothness parameter which plays an important role in the smoothness process. Here, we set adaptive smoothness parameters by

$$\omega_{ij} = \frac{K^2}{K^2+|\nabla p_i|^2}\cdot\lambda_{ij} \tag{7}$$

where $K=k_0\sigma_i^2$ is the noise level parameter [7], $|\nabla p_i|$ is the gradient magnitude of voxel p_i in the 3D projection domain and λ_{ij} is 1. In the implementation, the variance σ_i^2 and gradient $|\nabla p_i|$ are updated according to the new updated projection image per iteration.

IV. FDK-type Spectral CT Reconstruction

After the noisy spectral sinogram data are restored, a 3D-weighted helical FDK algorithm [8] is selected for analytic spectral CT reconstruction. It is an improved version of the first spiral CBCT algorithm [9]. The algorithm is implemented by assuming a flat panel detector, and a rebinning procedure is used to convert the cone-beam data into cone-parallel geometry. The algorithm can be expressed as

$$\hat{f}(x,y,z) = \int_{\theta_{\min}}^{\theta_{\max}}\omega_{3D}(\theta,t,\gamma)\tilde{P}^{PF}\left(\theta,t(x,y,z),v(x,y,z,\theta)\right)\mathrm{d}\theta, \tag{8}$$

where $[\theta_{\min},\theta_{\max}]\subset[\pi+2\beta_{\max},2\pi]$ is the view angle range over which the projection data are used to reconstruct an image slice intersecting the helical source trajectory at view angle $\theta_0=\theta_{\min}+(\theta_{\max}-\theta_{\min})/2$, and $\beta_{\max}$ is the half maximun fan angle of an x-ray beam. Projections $\tilde{P}^{PF}$ are gained by pre-weighting and filtering the parallelly rebinned projection P^{PF}

$$\tilde{P}^{PF}(\theta,t,v) = \left(\cos\gamma\cdot P^{PF}(\theta,t,v)\right)*h(t). \tag{9}$$

Here, θ is the view angle, t is the orthogonal distance from the iso-ray to parallel beam scanning geometry, and v is the row coordinate of projections on the detector,

$$t(x,y,\theta) = y\cos\theta - x\sin\theta, \tag{10}$$

$$v(x,y,z,\theta) = z\frac{R^2+DO\sqrt{R^2-t^2}}{R^2-t^2+b(x,y,\theta)\sqrt{R^2-t^2}}, \tag{11}$$

$$b(x,y,\theta) = x\cos\theta + y\sin\theta. \tag{12}$$

In Eq.(11), R is the source trajectory radius and DO is the distance from detector center to object center. In Eq.(9), the pre-weighted factor is

$$\cos\gamma = \frac{R^2+DO\sqrt{R^2-t^2}}{\sqrt{R^4+(b^2+DO^2)(R^2-t^2)+2R^2DO\sqrt{R^2-t^2}}}. \tag{13}$$

In Eq.(8), $\omega_{3D}(\theta,t,\gamma)$ is the 3D weighting function

$$\omega_{3D}(\theta,t,\gamma) = \frac{\omega_{2D}(\theta,t)\tan^{kh}(\gamma_c)}{\omega_{2D}(\theta,t)\tan^{kh}(\gamma_c)+\omega_{2D}(\theta\pm\pi,-t)\tan^{kh}(\gamma)}. \tag{14}$$

where γ and γ_c are the cone angles corresponding to a direct ray and its conjugate ray, respectively, h is the normalized helical pitch defined by $h=H/L$ with L being the height of the detector along the z-direction at the iso-centre, and k is a parameter varying over different helical pitches.

In Eq. (14), the 2D weighting function $\omega_{2D}(\theta,t)$ can be constructed in the case of cone-parallel geometry

$$\omega_{2D}(\theta,t)+\omega_{2D}(\theta\pm\pi,-t)=1, \tag{15}$$

where $\theta\pm\pi$ and $-t$ are the view angle and orthogonal iso-distance of the ray that is conjugate to the ray with view angle θ and orthogonal iso-distance t, respectively.

In Eq. (8), if we change the 3D weighting function into 2D weighting function $\omega_{2D}(\theta,t)$,we can gain the 2D-weighted helical FDK algorithm.

V. Reconstruction Results

A. Experimental Setting

To evaluate the performance of analytic reconstruction algorithm for spectral CT, a cylindrical phantom is designed to

include multiple materials. The diameter and height of the cylindrical are 20 cm and 10 cm, respectively. Its cross section is shown in Fig. 1. Assuming the center of this cylindrical is the origin of 3D coordinate system, we arrange 14 holes and each hole contains one material. While the objects 1-8 are used to evaluate the discriminative capability of spectral CT, the objects 9-14 are used to measure the spatial resolution of reconstructed images. The concentration percentages of base materials are calculated by weight and the linear attenuation coefficients of all the materials are shown in Fig. 2.

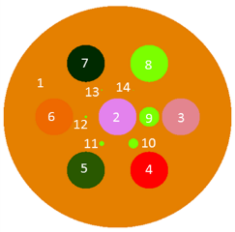

Fig. 1. Transaxial sketch of the cylindrical phantom.

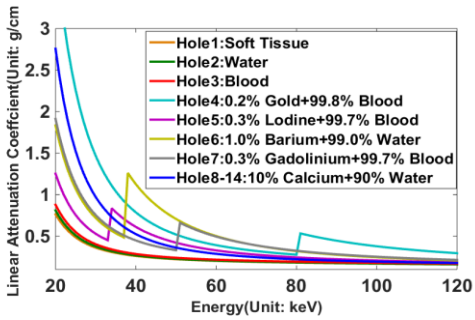

Fig. 2. Attenuation coefficients of 8 employed materials.

The x-ray tube voltage is assumed as 120kVp and the spectrum is shown in Fig 3. Taking into account the material k-edges in this phantom, which are iodine (33keV), barium (37.4keV), gadolinium (50.2keV) and gold (80.7keV), six channels are selected to make the total photons of each channel as equivalent as possible

$WE_1 = \{15.5\text{keV} \sim 32.5\text{keV}\}$, $WE_2 = \{33.5\text{keV} \sim 36.5\text{keV}\}$,

$WE_3 = \{37.5\text{keV} \sim 42.5\text{keV}\}$, $WE_4 = \{43.5\text{keV} \sim 49.5\text{keV}\}$,

$WE_5 = \{50.5\text{keV} \sim 56.5\text{keV}\}$, $WE_6 = \{81.5\text{keV} \sim 119.5\text{keV}\}$.

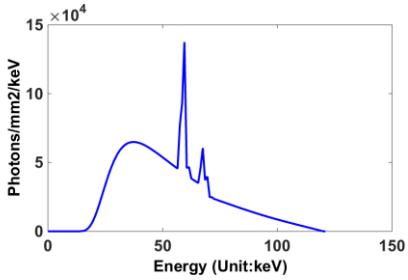

Fig. 3. Source photon emission spectrum used for numerical simulation.

To evaluate the weighted helical FDK algorithm for spectral CT, helical cone-beam data for each channel is simulated assuming a spectral CT geometry. The distance from the source to the center of the phantom is 75cm and the distance from the source to the detector is 15cm. The flat panel detector consists of 300×20 detector cells and each of which covers an area of 0.1×0.1cm^2. The phantom consists of 256×256×128 voxels. The photon count per ray is proportional to the source photon emission spectrum and the projections are collected according to Eq.(2). Here 360 projections are generated for one turn of the helical scanning. To evaluate the accuracy of the weighted FDK algorithm for higher helical pitch, the images which are reconstructed from noise-free sinogram with a low helical pitch of 0.5 in the cone-parallel geometry using no weighted helical FDK algorithm as reference.

B. 3D View Weighting versus 2D View Weighting

To evaluate the accuracy of the 3D weighted FDK algorithm for higher helical pitch, the 2D and 3D weighted FDK algorithms are employed and the projections are assumed noise-free. First and second rows of Fig. 4 are the transaxial and coronal images of the cylindrical phantom reconstructed from the 2D weighted helical FDK at 1, 3, 5th energy channels with a helical pitch of 1.5, and the third and fourth rows of Figure 4 are the corresponding images reconstructed by the 3D weighted helical FDK. Table 1 gives the normalized root mean squared error (NRMSE) and signal-noise-ratio (SNR) for different energy channels with 2D/3D weighted FDK at pitch 1.5.

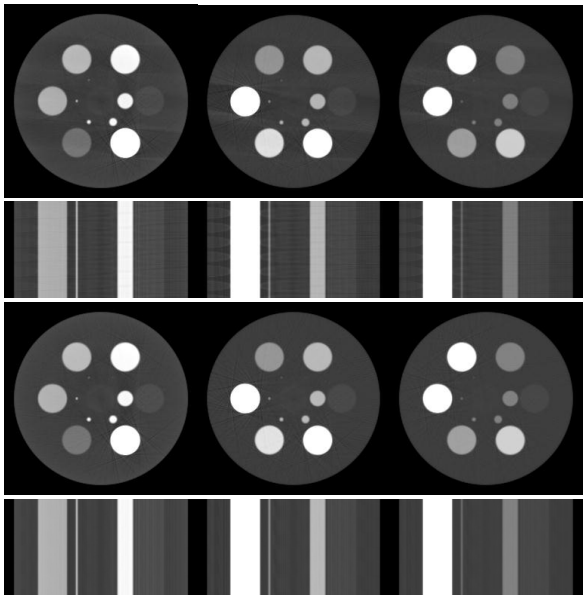

Fig. 4. Cylindrical phantom images reconstructed by the 2D/3D weighted helical FDK algorithms with a helical pitch of 1.5. From left to right columns, the images are reconstructed from 1st, 3rd ,5th channels. The first and second row images are respectively the transaxial and coronal planes of 2D view weighting results, and the third and fourth rows are the counterparts of 3D weighting results. The display window is [-500HU,1500HU]

TABLE I. NRMSE AND SNR OF RECONSTRUCTED IMAGES IN DIFFERENT CHANNELS WITH 2D/3D WEIGHTING FDK AT PITCH 1.5

channel	NRMSE		SNR	
	2D	*3D*	*2D*	*3D*
1	0.1824	0.0063	18.15	47.33
2	0.1820	0.0062	18.16	47.44
3	0.1788	0.0070	18.01	46.18
4	0.1825	0.0061	18.20	47.74
5	0.1835	0.0058	18.25	48.24
6	0.1897	0.0039	18.50	52.21

From Fig. 4, we can see that the shading artifacts of 2D weighted FDK is serious at high helical pitch. However, the 3D weighted FDK algorithm can suppress those shading artifacts and provide better reconstructed results at higher helical pitch. Table 1 further confirms the 3D weighted helical FDK algorithm is robust with respect to the helical pitch.

C. Noise Characterization

In practical applications, measurement noise is unavoidable. To test the noise characterization of the 3D weighted helical FDK algorithm against data noise, Poisson noises are generated with the expectation being the corresponding received noise-free photon numbers.

Table 2 gives the corresponding NRMSE and SNR of the reconstructed images from noisy and denoised sinograms. From Table 2, we can see that the photon noise has greater influence to lower energy channels compared to higher energy channels. Fig.5 gives the transaxial images in the first three energy channels reconstructed from denoised sinograms by using the aforementioned adaptive MAP method with helical pitches of 1.5. Table 2 and Fig. 5 show that the analytic spectral CT reconstruction is stable with respect to noisy sinograms. We also can see that the results reconstructed from denoised sinograms have lower NRMSE and higher SNR compared to the ones from noisy sinograms.

TABLE II. NRMSE AND SNR IN DIFFERENT CHANNELS WITH 3D WEIGHTING FDK AT PITCH 1.5 FROM NOISY PROJECTIONS

channel	NRMSE		SNR	
	Noise	*Denoise*	*Noise*	*Denoise*
1	0.0219	0.0182	36.56	38.15
2	0.0149	0.0128	39.91	41.19
3	0.0112	0.0104	42.06	42.68
4	0.0087	0.0083	44.67	45.09
5	0.0082	0.0079	45.20	45.60
6	0.0061	0.0058	48.33	48.84

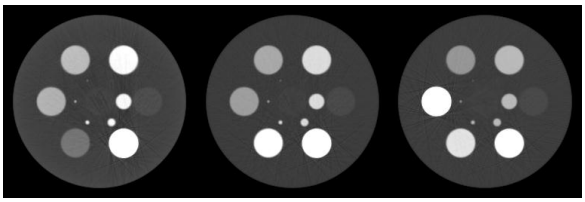

(a) (b) (c)

Fig. 5. Transaxial images reconstructed from denoised projections with a helical pitch of 1.5. (a)-(c) are reconstructions from the first three energy channels. The display window is [-500HU,1500HU].

VI. DISCUSSION AND CONCLUSION

In this paper, we mainly focus on the evaluation of an analytic reconstruction algorithm for spectral CT with high helical pitches. First, an adaptive MAP sinogram restoration statistical algorithm is used for denoising in the projection domain. Then, a 3D weighted helical FDK algorithm is used to reconstruct the spectral CT images, and satisfactory reconstruction accuracy is achieved with high pitches. While the 2D weighted FDK can be used to deal with half-scan and full scan problem, 3D weighted FDK can significantly improve the reconstruction accuracy at larger helical pitch, and the reconstruction accuracy of 3D weighted FDK depends on the parameters k in Eq. (14). Generally speaking, a greater value of k should be set for a large helical pitch. In our numerical simulations, k is empirically selected as 30 for pitches 1.5. Because spectral CT can capture more information in different spectral channels simultaneously, it can provide much richer information rather than the traditional gray-scale CT.

In conclusion, we have evaluated an analytic helical reconstruction approach for spectral CT. Because this approach is fast and it can provide high spatial resolution, high contrast resolution and high SNR with higher helical pitches, it can serve as a platform to evaluate the state-of-the-art iterative spectral CT algorithms. We are working to link this platform with the new data format developed by Dr. McCollough's group at Mayo Clinic, and the corresponding software package will be released soon. The numerical results have confirmed the merits of analytic spectral CT reconstruction in terms of both qualitatively and quantitatively analysis.

Acknowledgment

This work was partially supported by grants from U.S. National Institute of Biomedical Imaging and Bioengineering in terms of a U01 projection (EB017140) and the National Science Foundation of China (No. 61601412, 61571404).

References

[1] Y. Xi, Y. Chen, R. Tang, J. Sun and J. Zhao, "United iterative reconstruction for spectral computed tomography," IEEE Trans. Med. Imag., Vol. 34, pp. 769-778, Mar. 2015.

[2] L. Li, Z. Chen, W. Cong and G. Wang, "Spectral CT Modeling and Reconstruction with Hybrid Detectors in Dynamic-Threshold-Based Counting and Integrating Modes," IEEE Trans. Med. Imag., Vol. 34, pp. 716-728, Mar. 2015.

[3] P. He, H. Y. Yu, J. Bennett, P. Ronaldson, R. Zainon, A. Butler, P. Butler, B. Wei and G. Wang, "Energy-discriminative performance of a spectral micro-CT system," Journal of X-ray science and technology, Vol. 21, pp. 335-345, 2013.

[4] H. Yu, Q. Xu, P. He, et. al, "Medipix-based spectral Micro-CT," CT Theory and Applications, Vol. 21, pp. 583-596, Dec. 2012.

[5] Y. Zhang, J. Zhang, and H. Lu, "Statistical sinogram smoothing for low-dose CT with segmentation-based adaptive filtering," IEEE Trans. Nuc. Sci. Vol. 57, Oct. 2010.

[6] J. Wang, T. Li, H. Lu, and Z. Liang, "Penalized weighted least-squares approach to sinogram noise reduction and image reconstruction for Low-Dose X-ray computed tomography," IEEE Trans. Med. Imag., Vol. 25, pp.1272-1283, Otc. 2006.

[7] X. Cui, Q. Zhang, H. Shangguan, Y. Liu and Z. Gui, "The asaptive sinogram restoration algorithm based on anisotropic diffusion by energy minimization for low-dose X-ray CT," Optik, Vol. 125, pp. 1694-1697, 2014.

[8] X. Tang, J. Hsieh, R. A. Nilsen, S. Dutta, D. Samsonov, and A. Hagiwara, "A three-dimensional-weighted cone beam filtered backprojection (CB-FBP) algorithm for image reconstruction in volumetric CT—helical scanning," Phys. Med. Biol., vol. 51, pp. 855-874, Feb. 2006.

[9] G. Wang, T. H. Lin, P. C. Cheng, D.M. Shinozaki, "A general cone-beam reconstruction algorithm," IEEE Trans. Med. Imag., Vol. 12, pp. 486-496, Sep. 1993.